Green Chemistry

Accepted Manuscript

This article can be cited before page numbers have been issued, to do this please use: M. K. Bayazit, E. Cao, A. Gavriilidis and J. Tang, *Green Chem.*, 2016, DOI: 10.1039/C5GC02245B.

ROYAL SOCIETY OF CHEMISTRY

www.rsc.org/greenchem

View Article Online
DOI: 10.1039/C5GC02245B

Microwave Promoted Continuous Flow Approach to Self-assembled Hierarchical Hematite Superstructures

M. K. Bayazit, E. Cao, A. Gavriilidis and J. Tang*

Department of Chemical Engineering, University College London, Torrington Place, London, WC1E 7JE, UK

Abstract

In this work a microwave promoted flow (MWPF) system to reproducibly synthesize self-assembled hierarchical hematite superstructures (Hem-SSs) using sole precursor ($Fe(NO_3)_3.9H_2O$) and single mode microwave in aqueous conditions has been developed. The functional characterisation by XRD, (HR)TEM, XPS, UV-vis and Raman spectroscopies proved that highly crystalline ellipsoid Hem-SSs (~180 nm × 140 nm) were produced, built from primary hematite nanoparticles, 5–10 nm in size using 0.05 mol L^{-1} precursor concentration, 1 mL min^{-1} flow rate and short reaction time (about 6 min). Particles produced via conventional heating (CH) at 120 and 140 °C in the same flow reactor under similar experimental conditions were found to consist of mixtures of goethite and hematite. The effects of precursor concentration (0.1 and 0.2 mol L^{-1}) and flow rate (2 and 5 mL min^{-1}) on Hem-SSs were further investigated and the synthesis mechanism was also discussed. This novel method opens a window for continuous fabrication of metal or metal oxide nanoparticles/superstructures by a green approach to meet industrial requirement.

View Article Online
DOI: 10.1039/C5GC02245B

Introduction

Highly-ordered superstructures, so-called mesocrystals, formed via hierarchical self-assembly of primary nanoparticles (NPs) following a non-classical crystallization route are interesting materials due to their distinctive properties including enhanced surface area, accessible pores and tunable electronic, optical and magnetic properties that make them potentially applicable in catalysis, paints, sensors and electronics.[1-4] Metal oxide superstructures have recently been reviewed, with particular attention on their use for energy conversion and storage applications.[5] Among them, highly oriented hematite superstructures (Hem-SSs) have attracted specific attention due to their excellent lithium insertion,[6, 7] photocatalytic performance[8] and improved sensing properties[9] compared to hematite single crystals.

Platelike α-Fe_2O_3 mesocrystals were used as a support to prepare gold loaded platelike α-Fe_2O_3 mesocrystals that were shown to be highly efficient and stable catalyst for CO conversion compared to commercially available α-Fe_2O_3 sample (Fluka).[9] Higher activity was attributed to the significant increase in the (110) diffraction intensity for the platelike α-Fe_2O_3 mesocrystal support.[9] Furthermore, high temperature (400 °C) annealed platelike α-Fe_2O_3 mesocrystals showed enhanced gas-sensing sensitivity compared to commercial α-Fe_2O_3, probably due to highly-oriented and crystalline α-Fe_2O_3 superstructures.[9] Similarly, as-prepared rhombic α-Fe_2O_3 mesocrystals were tested for lithium storage capacity that demonstrated improved cycling stability for 5-50 cycles with storage capacity of 756 mA h g^{-1} after 50 cycles, probably due to the closed and intracrystalline porosity, compared to single-crystal α-Fe_2O_3 that showed gradual loss of capacity after ~20 cycles.[6]

Hematite is an n-type semiconductor (E_g=2.1 eV) with rhombohedral crystal structure and is weakly ferromagnetic at room temperature.[10] Hematite (α-Fe_2O_3) as a precursor can also be converted into other useful forms of iron oxide such as maghemite (γ-Fe_2O_3) and magnetite (Fe_3O_4).[11] Hematite nanoparticles (Hem-NPs) can be synthesized conventionally by several

View Article Online
DOI: 10.1039/C5GC02245B

techniques including hydrothermal/solvothermal,[12, 13] sol-gel processing[14] and chemical vapor deposition methods,[15] using predominately a batch reactor or a large tubular reactor. Alternatively, a microwave-assisted hydrothermal batch reactor can be employed to prepare nanosized hematite particles as catalysts and adsorbents using both $Fe(NO_3)_3$ (0.1 mol L^{-1}) and urea (0.5 mol L^{-1}) as precursors.[16]

Mesocrystals or superstructures of hematite can be prepared by a complicated self-assembly of primary hematite nanoparticles. In these processes, organic surfactants or templates are crucial to form surface stabilized primary Hem-NPs that prevent particle-particle fusion during mesocrystal formation. However, these additives are likely to decompose into hazardous materials at high reaction temperatures and long reaction times.

For example, porous plate-like hematite mesocrystals with a dimension of 100-400 nm were synthesized by self-assembly of *in-situ* prepared Hem-NPs (5-15 nm) in an ionic liquid [Bmim]Cl, acting as both solvent and templating agent, via a controlled solvent evaporation process reacting $FeCl_3.6H_2O$, water and *n*-butylamine in air at 120 °C for 20 h.[9] Similarly, olive-like photocatalytically active Hem-SSs with size 620 nm × 940 nm have recently been prepared via self-assembly of primary hematite nanoparticles (5-10 nm) using $FeCl_3$ and silk fibroin as a biotemplate in water by heating at 160 °C for 10 h.[8] A solvothermal approach was used to prepare high-stability hematite mesocrystals from $Fe(NO_3)_3.6H_2O$ in *N,N*-dimethylformamide (DMF) and methanol (MeOH) mixture with varying amounts at 180 °C for 24 h.[6] It was proposed that the intermediate $NH_2(CH_3)_2^+$ acted as stabilizer for primary hematite particles and higher amount of methanol conditions produced rhombic (DMF:MeOH; 20:5, v/v) or ellipsoidal (DMF:MeOH; 17:8, v/v) mesocrystals. A hydrothermal method at 200 °C for 12 h in ethanol/water mixture (9:1, v/v) to synthesize elliptic single-crystalline hematite superstructures was also reported.[7]

View Article Online
DOI: 10.1039/C5GC02245B

Although the abovementioned methods had their own advantages (*e.g.* controlling shape and growth direction of superstructures *etc*.) they obviously required additional chemicals (*e.g.* reducing agents, surfactants, templates or stabilizers). Furthermore, it is challenging to scale those processes up while retaining the same structure/properties due to long reaction times, limited reactor capacity, high-energy consumption and low product yields. To meet the increasing demand in highly stable, self-assembled, hierarchical superstructures with defined shapes for diverse applications, a green, reproducible and energy/cost efficient technique is desirable, which is also scalable. For this purpose, microwave heating (MH) coupled with continuous flow synthesis may offer an attractive route for the rapid, continuous and controlled growth of self-assembled stable metal oxide superstructures. The use of continuous micro/milliflow technology has gained significant attention in recent years owing to large surface-to-volume ratio that depresses the diffusion times of chemical species.[17-21] Microfluidic systems have been successfully utilized with CH to carry out chemical reactions and nanocrystal preparation due to their versatility to perform rapid mixing, controllable mass and heat transfer under continuous flow conditions.[17] Local variations in reaction conditions such as concentration, temperature and reaction time are likely to have significant effect on both nucleation and particle growth, and a better control over these variables may improve the monodispersity, particle size and its distribution, shape and morphology, crystallinity and purity of nano-particles manufactured, which MH could provide due to its fast and selective heating.

Herein, continuous manufacturing of self-assembled hierarchical ellipsoid hematite superstructures (Hem-SSs) with an average dimension of ~100-200 nm using a microwave promoted continuous flow approach in an aqueous solution using $Fe(NO_3)_3.9H_2O$ as the only precursor is presented for the first time. The effect of precursor concentration and flow rate on the geometry and morphology of the formed particles were investigated. The results

View Article Online
DOI: 10.1039/C5GC02245B

obtained by MH were also compared with the results of particles produced by CH under similar reaction conditions. Furthermore, the reproducibility of the process was examined.

Experimental

Synthesis of Hematite Nanoparticles. All chemicals were purchased from Sigma-Aldrich and used as received. The microwave promoted continuous flow method consisted of a flow reactor (6 mL) made of 1/8" PTFE tubing, a CEM single-mode microwave system, a syringe pump, a temperature probe positioned at the exit of reactor, a sample/waste collection unit with backpressure regulator and an ice-bath. For the synthesis of particles using CH, the microwave instrument was replaced by a thermal bath using glycerol as a heating medium. In a typical procedure, a 50 mL syringe filled with 0.1 mol L^{-1} of iron (III) nitrate nonahydrate ($Fe(NO_3)_3.9H_2O$, 99.9%) solution (pale yellow in color) dissolved in deionized water at room temperature was connected to the flow reactor and the reactor was filled with the precursor solution. The pressure of the flow reactor was adjusted at 20 psi using a pressurized air cylinder. Pressure adjustment was provided via air controlled by a pressure regulator (20 psi) with a gas escape route immersed in a water bath. The precursor was pumped into the flow reactor at a flow rate of 1 mL min^{-1} and pre-adjusted microwave irradiation (40 W) was applied simultaneously. After 8 min, the temperature probe displayed a constant temperature value (~119-120 °C) and 8 mL of the pumped solution was collected in waste collection unit. Thereafter, the main product mixture passed through an ice-bath to cool down below room temperature and was collected in a sample collection unit. The mixture was centrifuged at 2500 rpm for 90 min to recover the particles formed. Recovered particles were washed by deionized water and re-centrifuged, isolated and dried at room temperature for characterization.

Materials Characterization. The X-ray diffraction (XRD) patterns of samples were obtained with a Bruker D8 Advance Powder X-ray diffractometer with a Mo-K_α (λ=0.71 Å) radiation

View Article Online
DOI: 10.1039/C5GC02245B

source. Diffraction patterns were collected from 10° to 70° and a step size of 0.002 °/s was used. Field emission scanning electron microscopy (FESEM) was employed to observe the size and shape of the nanomaterials, using a JEOL JSM-7401F operating at 3-5kV. Materials were tested in powder form prepared from ethanol dispersions. UV/Vis spectra were obtained from stable dispersions of produced particles in ethanol using a Shimadzu UV-2550 UV/Vis spectrophotometer. High-resolution XPS was performed by a Thermo Scientific K-alpha photoelectron spectrometer with monochromatic Al-K_α radiation; peak positions were referenced to C 1s line at 284.5 eV and the CasaXPS software was used for data processing. Transmission electron microscopy (TEM) and high resolution transmission electron microscopy (HRTEM) were performed using Jeol JEM-1010 and JEOL-2010F coupled with an EDS detector (Oxford Instruments) instruments, respectively. TEM samples were prepared from stable dispersions of particles prepared in ethanol by dropping on carbon coated copper grids. Particle size distribution was estimated from TEM data measuring particle size using ImageJ. All graphs and statistical analysis were obtained by OriginLab software (Origin9.1).

Results and discussion

Preparation of HEM-SSs. Highly pure and crystalline Hem-SSs, reddish-brown in color, were successfully fabricated via a cheap and readily available precursor, $Fe(NO_3)_3.9H_2O$, under flow conditions. Unlike previously reported conventional and microwave-assisted hydrothermal batch processes,[6, 8, 9, 16] MWPF synthesis of Hem-SSs does not require any reducing agent (*e.g.* urea), surfactant or template. The potential by-products have a high solubility in water (e.g. HNO_3), facilitating the isolation/purification of synthesized ellipsoid Hem-SSs, thus low speed centrifugation was applied. Hem-SSs were produced at 120 ^oC under 40 W fixed MW power, 1 mL min^{-1} flow rate and 20 psi applied back pressure. It is also worth noting that the temperature value (120 ^oC) was recorded outside the MH zone using a temperature probe positioned *ca.* 5 cm away from the reactor exit from the

View Article Online
DOI: 10.1039/C5GC02245B

microwave irradiated zone. Thus, the inside temperature of the flow reactor is likely to be somewhat higher than that of the recorded temperature outside the microwave cavity. The current configuration of the reactor and small microwave cavity make the measurement of the temperature of hot fluid inside the reactor very difficult. In order to make our comparison more accurate, we estimated the temperature at the exit of the microwave irradiated zone, taking into account the heat transfer between the fluid inside the PTFE tubing and the outside surrounding air (**See ESI for calculations**). The estimated fluid temperatures at the exit of the microwave irradiated zone for different fluid flow rates are listed in Table 1. It can be seen that the temperature difference between the inside temperature near the exit and the measured is quite small, less than 7 ^{o}C at the current conditions.

Table 1 Estimated fluid temperature at the exit of the microwave irradiated zone

Fluid volume flow rate (F), mL min^{-1}	Fluid mass flow rate (m), g s^{-1}	Temperature at the exit of the microwave irradiated zone ($t_{i,MW}$), °C
1	0.01663	126.7
2	0.03327	123.3
5	0.08317	121.3

The X-ray diffraction (XRD) patterns of iron oxide particles prepared by the MWPF system using different concentrations (0.05, 0.1 and 0.2 mol L^{-1} precursor) show the presence of characteristic hematite (α-Fe_2O_3) peaks (**Figure 1a**). In contrast, an inseparable mixture with poor crystallinity, attributed to the mixture of hematite and goethite particles indicated by XRD, was obtained when the reaction was conducted by CH using 0.1 and 0.2 mol L^{-1} $Fe(NO_3)_3.9H_2O$ precursor concentrations at 120 °C and even 140 °C (not shown) (**Figure 1a**). When the precursor concentration was decreased to 0.05 mol L^{-1} $Fe(NO_3)_3.9H_2O$, no particles were isolated when reaction was performed by CH at 120 °C. On the other hand, highly pure and crystalline hematite particles were obtained (confirmed by sharp and narrow XRD peaks) when 0.05 M $Fe(NO_3)_3.9H_2O$ precursor was used (**Figure 1a**). The observed XRD peaks for Hem-SSs (ICSD—96075) were assigned to Miller's indices of [012], [104],

View Article Online
DOI: 10.1039/C5GC02245B

[110], [113], [202], [024], [116], [018], [214], [300], [208], [1010], [220], [306], [223], [312], [0210], [134], [315] and [2110]. When high concentration of precursor (0.1 and 0.2 mol L^{-1} $Fe(NO_3)_3.9H_2O$) was used, Hem-SSs were again produced successfully. However, slightly broadened XRD peaks were observed, suggestive of less crystalline hematite particle formation possibly due to insufficient microwave energy provided. XRD results reveal that the degree of crystallinity of the MWPF system synthesized Hem-SSs was related to the precursor concentration. Low precursor concentrations yielded highly crystalline hematite preparation.

The oxidation state of Fe in Hem-SSs prepared by MWPF using 0.05 mol L^{-1} $Fe(NO_3)_3.9H_2O$ precursor was further analyzed by XPS. Previous studies for α-Fe_2O_3 reported two main peaks positioned at *ca.* 724 and 711 eV, attributed to Fe $2p_{1/2}$ and Fe $2p_{3/2}$, respectively.[22] It was also shown that the latter one was narrower and stronger[23] and these peaks were clearly accompanied by satellite structures on their high binding-energy side, at about 8 eV.[22] Consistent with previous literature, XPS analysis of Hem-SSs displayed four peaks at *ca.* 733, 724, 719 and 711 eV, confirming the synthesis of pure hematite structures (**Figure 1b**).

View Article Online
DOI: 10.1039/C5GC02245B

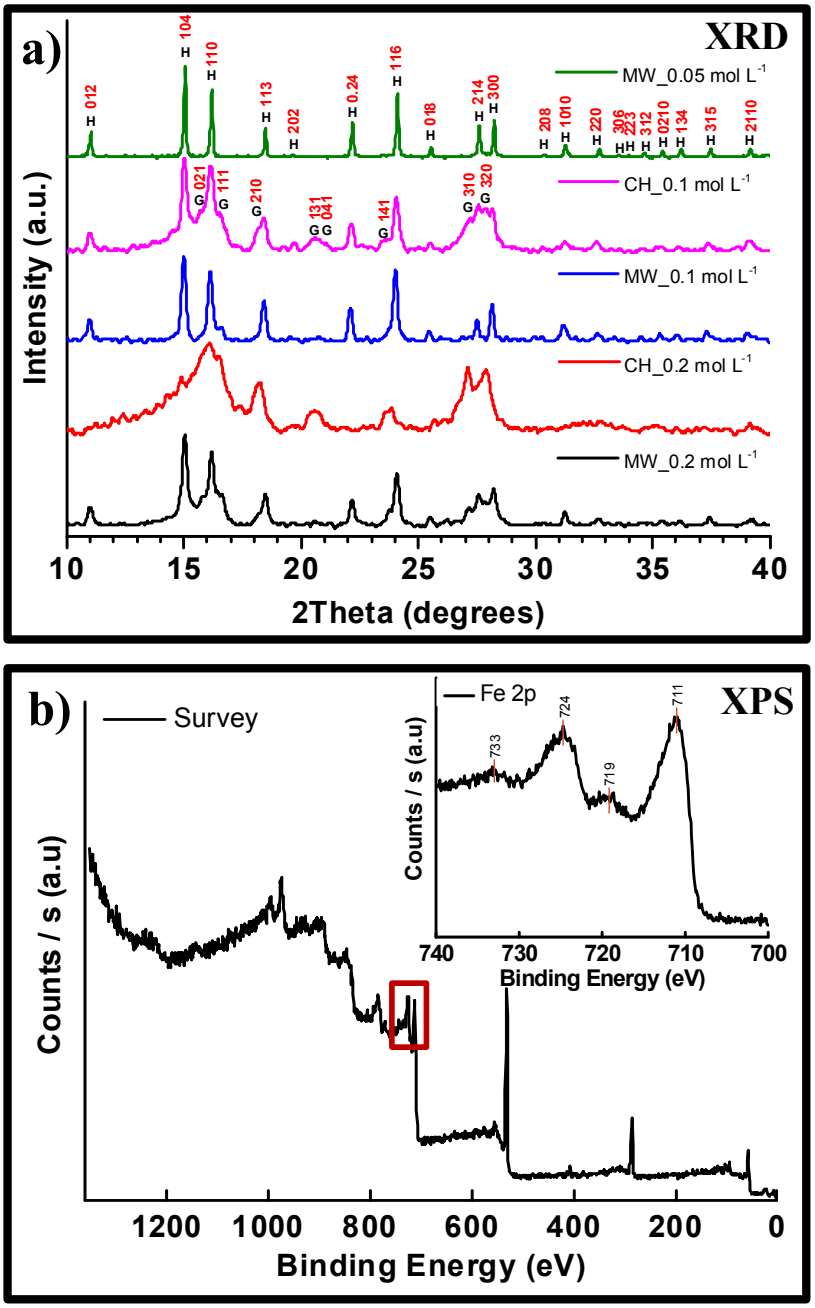

Figure 1 (a) XRD patterns of MH and CH assisted flow system synthesized particles at 120 °C using 0.05, 0.1 and 0.2 mol L^{-1} $Fe(NO_3)_3.9H_2O$ precursor. Molybdenum K-alpha (λ=0.71 Å) was used as a source. 'G' corresponds to goethite. **(b)** XPS spectrum of MWPF synthesized Hem-SSs at 1 mL min^{-1} flow rate (Reactor volume: 6 mL) using 0.05 mol L^{-1} $Fe(NO_3)_3.9H_2O$ precursor. Inset: Expanded Fe 2p XPS spectrum of Hem-SSs.

View Article Online
DOI: 10.1039/C5GC02245B

Absorption spectroscopy has been widely used to characterize hematite particles in solution and solid state.[23, 24] As expected, UV-vis spectra of isolated Hem-SSs show an absorption band at *ca.* 390 nm and a weak shoulder at *ca.* 530 nm, characteristic of pure hematite, compared to $Fe(NO_3)_3.9H_2O$ precursor (**Figure 2**).

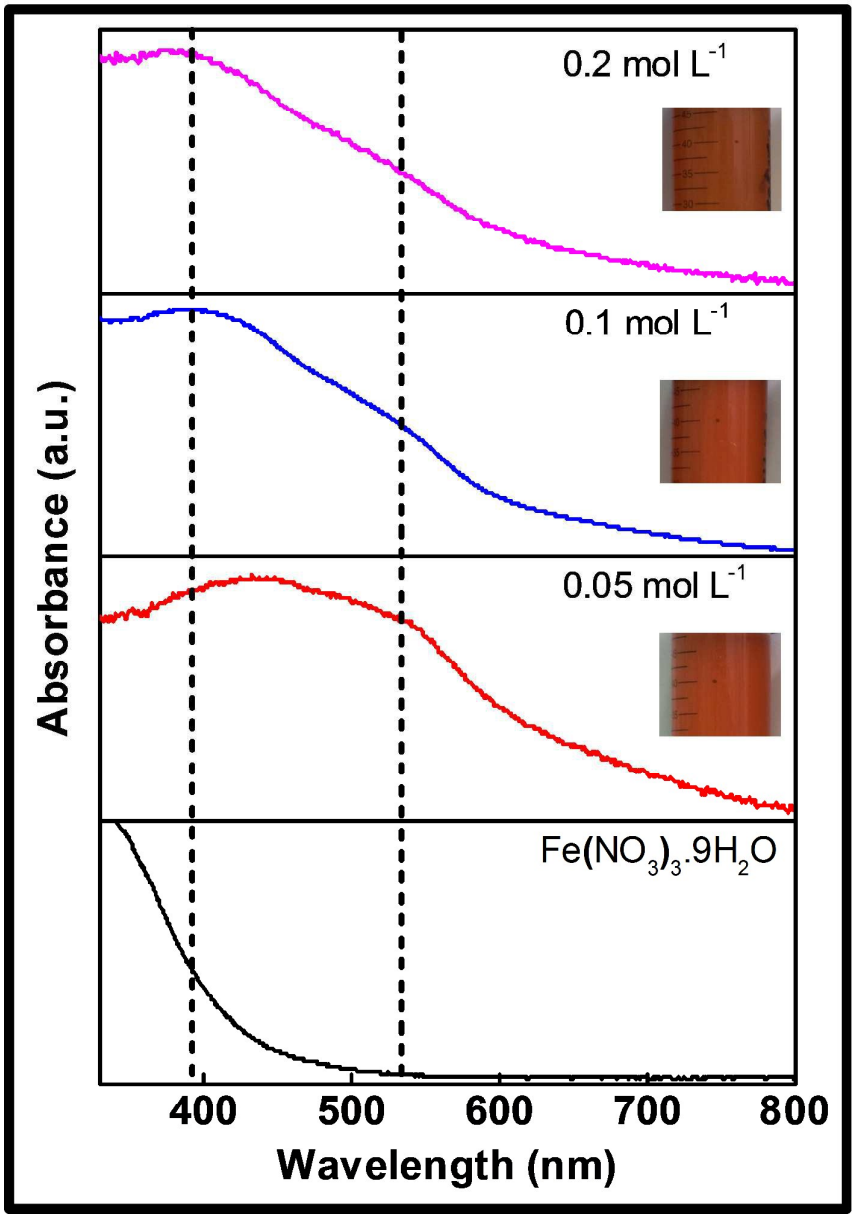

Figure 2 Photos and absorption spectra of MWPF system synthesized Hem-SSs using 0.05, 0.1 and 0.2 mol L^{-1} $Fe(NO_3)_3.9H_2O$ precursor, and pure $Fe(NO_3)_3.9H_2O$ precursor.

View Article Online
DOI: 10.1039/C5GC02245B

Furthermore, it was noticed that the characteristic absorption bands of Hem-SSs prepared by 0.05 mol L^{-1} $Fe(NO_3)_3.9H_2O$ precursor were red-shifted by ~20 nm compared to 0.1 and 0.2 mol L^{-1} precursor concentration. Although this type of shift is generally attributed to larger particle size, it may also be due to high crystallinity of the produced particles using 0.05 mol L^{-1} precursor, coinciding with XRD patterns of these samples.[25] Conversely, no clear hematite related absorption band was observed for the isolated particles produced by CH at 120 ^oC using 0.1 mol L^{-1} $Fe(NO_3)_3.9H_2O$ precursor in a flow reactor although XRD pattern (please see Figure 1a) of isolated particles revealed a mixture of goethite and hematite particles (**ESI Figure S1**). On the other hand, consistent with observed XRD peaks, the isolated particles produced by CH at 120 ^oC using 0.2 mol L^{-1} $Fe(NO_3)_3.9H_2O$ precursor showed an absorption band at *ca.* 400 nm, probably due to the presence of relatively high concentration of hematite particles in isolated mixture, compared to 0.1 mol L^{-1} $Fe(NO_3)_3.9H_2O$ precursor. Assuming that the temperature of the reactor in the microwave cavity was somewhat higher than 120 ^oC as predicted by our calculations, the reaction was further performed by CH at 140 ^oC using 0.1 mol L^{-1} $Fe(NO_3)_3.9H_2O$ precursor. However, no characteristic hematite related UV-vis absorption bands at *ca.* 390 and 530 nm were obtained, suggesting that pure hematite particles could not be prepared by CH at 120 and 140 ^oC under similar experimental conditions (**ESI Figure S1**). All these are consistent with results obtained by XRD measurements.

Transmission electron microscopy (TEM) provided insight into the morphology, particle size distribution and sub-units of Hem-SSs. TEM images of hematite particles prepared using 0.05, 0.1 and 0.2 mol L^{-1} $Fe(NO_3)_3.9H_2O$ show ellipsoid hematite structures with particle size (length/width) distribution of 180±92 nm/140±67 nm, 124±62 nm/75±33 nm and 112±69 nm/73±34 nm, respectively (**Figure 3a-f**). Close inspection of TEM image of ellipsoid hematite particles reveals that each particle has relatively rough surfaces and is composed of

View Article Online
DOI: 10.1039/C5GC02245B

highly oriented or self-assembled primary hematite particles, with boundaries between them (**Figure 3g**). The presence of clear particle-particle boundaries suggest that subunits of Hem-SSs are not fused and they might be dispersed by applying external forces (*e.g.* sonication, mechanical stirring *etc.*).

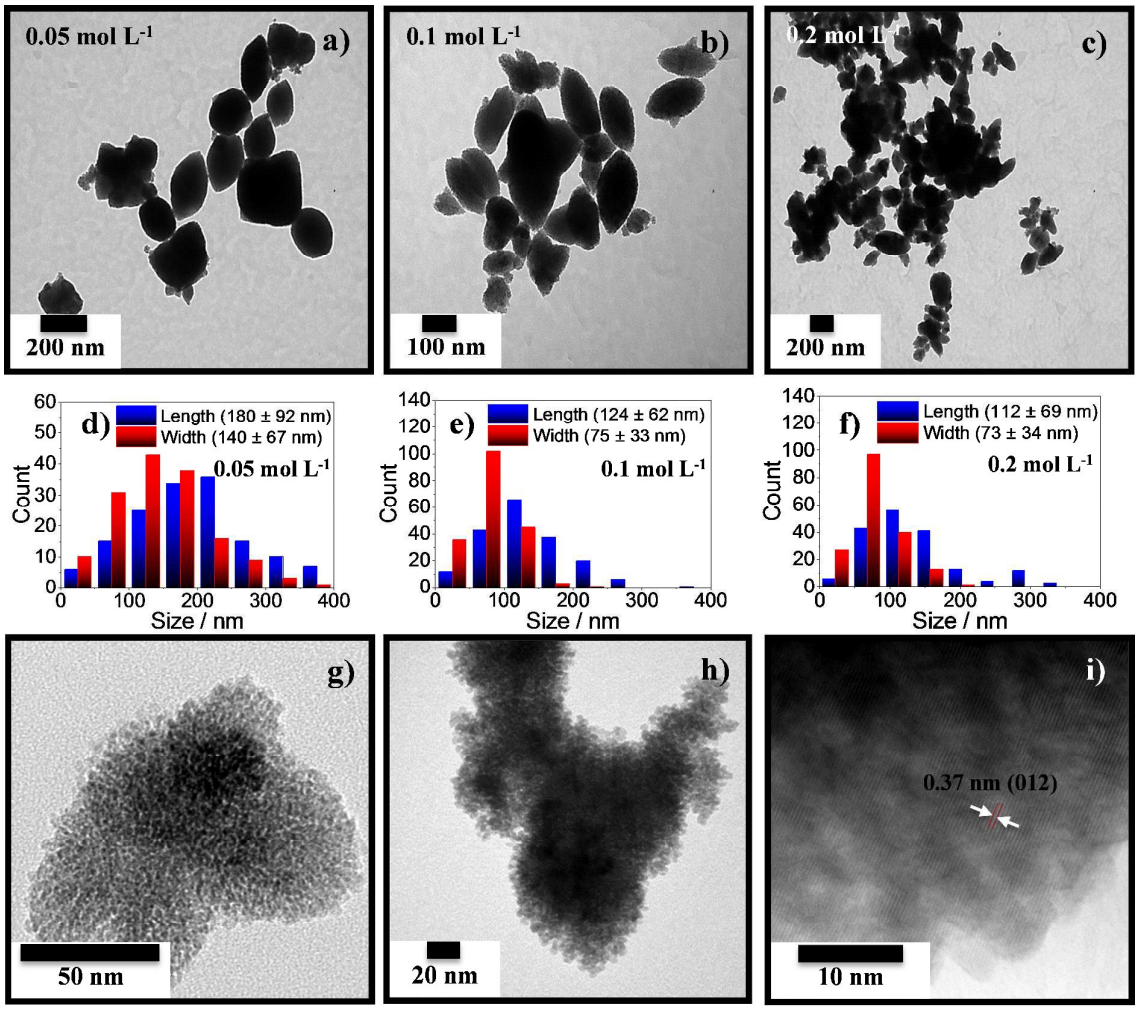

Figure 3 TEM images of MWPF system synthesized ellipsoid Hem-SSs using 0.05, 0.1 and 0.2 mol L^{-1} $Fe(NO_3)_3.9H_2O$ precursor and (**a-c**) particle size distribution (length/width) of ellipsoid Hem-SSs (**d-f**). TEM images of MWPF synthesized ellipsoid Hem-SSs before (**g**) and after (**h**) mild sonication using 0.05 mol L^{-1} $Fe(NO_3)_3.9H_2O$ precursor. HRTEM image of ellipsoid Hem-SSs using 0.05 mol L^{-1} $Fe(NO_3)_3.9H_2O$ precursor (**i**).

View Article Online
DOI: 10.1039/C5GC02245B

Thus, mild sonication (750 W sonic probe, 40% amplitude) was applied to ellipsoid Hem-SSs in ice cooled ethanol for 5 min. High-resolution TEM (HR-TEM) images of mildly sonicated Hem-SSs show partial exfoliation of uniform granular primary hematite nanocrystals approximately 5-10 nm in size (**Figure 3h**), suggesting that interaction between the subunits is relatively strong. Furthermore, it is worth noting that the ellipsoid morphologies of Hem-SSs are preserved, suggestive of highly-ordered stable superstructure. The lattice fringes in a typical HRTEM image (**Figure 3i**) are separated by ~3.7 Å, which agrees well with the [012] lattice spacing of hematite and further confirm that α-Fe_2O_3 NPs (*e.g.* crystallinity) are not altered via mild sonication. It is also worth noting that HRTEM analysis of α-Fe_2O_3 mesocrystals prepared by conventional heating in previous literature using both $Fe(NO_3)_3.9H_2O$[6] and $FeCl_3.6H_2O$[9] exhibited lattice fringes separated by ~2.5 Å, attributed to [110] facet as compared to Hem-SSs with [012] facet prepared by MWPF system. This probably suggests that microwave heating induces crystal growth along the [012] direction. It is therefore believed that mesocrystals prepared by MWPF system may show unusual activities due to their different crystal facet and lattice spacing that may provide more accessible surface compared to conventionally prepared mesocrystals.[6, 9] On the other hand, no ellipsoid pure hematite was observed by TEM analysis of particles prepared by CH (**ESI Figure S2**). HRTEM image of samples showed ~10 nm particles with irregular shapes and lattice spacing of ~2.0, 2.4 and 2.7 Å, corresponding to [131] lattice spacing of goethite, and [104] and [110] lattice spacing of hematite, respectively, further confirming that CH mainly produced a mixture of hematite and goethite nanoparticles. Overall (HR)TEM analysis of Hem-SSs suggests that MWPF system is able to produce highly stable and ordered Hem-SSs.

Effect of Reactant Flow Rate on Synthesis of Hem-SSs. The effect of reactant flow rate on the physical properties of the particles was studied by TEM, UV-vis and Raman spectroscopy. Typical reaction conditions (120 °C, 0.1 mol L^{-1}, 6 mL reactor) and applied

View Article Online
DOI: 10.1039/C5GC02245B

back pressure (20 psi) were kept constant and the reaction was carried out at flow rates of 1, 2 and 5 mL min^{-1}, where 1 mL min^{-1} was the minimum reliable flow rate in the current configuration. No visible particle formation was observed at 2 and 5 mL min^{-1} flow rates. Thus, the isolated hematite particles for 1 mL min^{-1} flow rate and soluble crude mixtures for 2 and 5 mL min^{-1} flow rates were used for bulk UV-vis and Raman analysis. UV-vis spectrum of the isolated particles synthesized at 1 mL min-1 flow rate showed the characteristic hematite absorption bands while

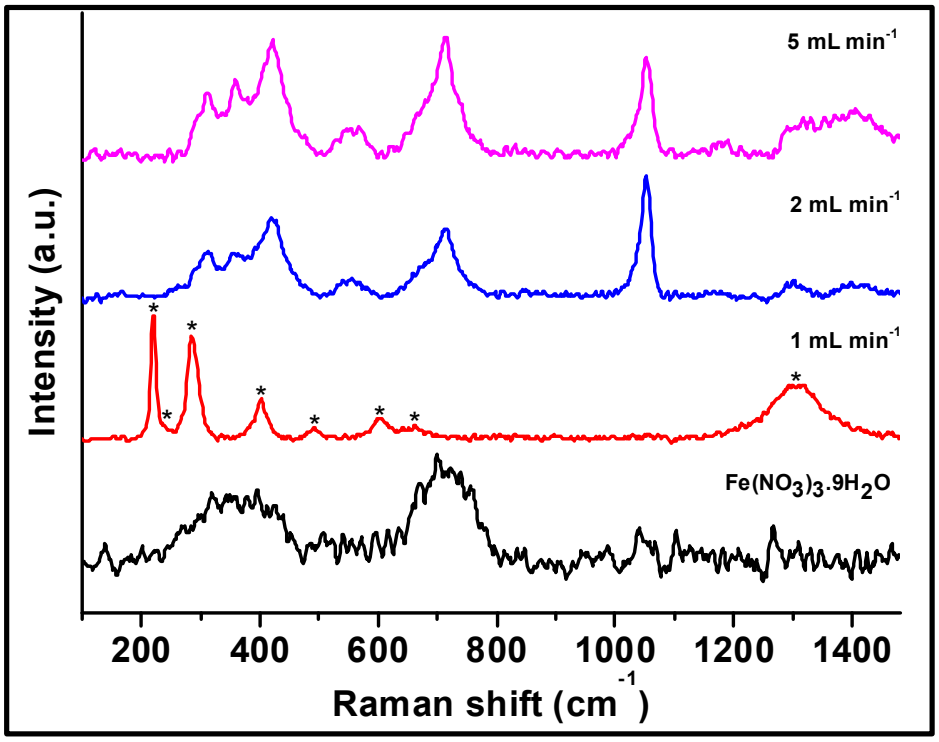

Figure 4 Raman spectra of MWPF system synthesized ellipsoid Hem-SSs using 0.05 mol L^{-1} $Fe(NO_3)_3.9H_2O$ precursor at 1, 2 and 5 mL min^{-1} flow rate, and pure $Fe(NO_3)_3.9H_2O$ precursor for comparison. * corresponds to the characteristic hematite related Raman shifts.

the crude mixtures prepared at higher flow rates showed no clear bands (**ESI Figure S3**). In agreement with previous literature,[26, 27] Raman spectra of Hem-SSs prepared via 1 mL min^{-1} flow rate displayed characteristic hematite (α-Fe_2O_3) Raman shifts at *ca.* 201, 240, 285, 401,

View Article Online
DOI: 10.1039/C5GC02245B

492, 601, 665 and 1300 cm^{-1}, compared to precursor signals positioned at 356 and 712 cm^{-1} (**Figure 4**). In contrast, reaction mixtures obtained at 2 and 5 mL min^{-1} flow rates showed no hematite related Raman shifts, suggesting that low residence times (3 min for 2 mL min^{-1} and 1.2 min for 5 mL min^{-1}) were not enough to produce hematite particles (**Figure 4**). Further TEM analysis of crude reaction product (2 mL min^{-1} flow rate) showed a mixture of small particles 1-2 nm in size, some ellipsoid (~200 nm in length) and spherical (~100 nm or less) particles, suggesting that the minimum residence time required to prepare pure ellipsoid Hem-SSs should probably be at *ca.* 6 min (1 mL min^{-1}) under the experimental conditions utilized (**ESI Figure S4**). Furthermore, no ellipsoid particle formation was observed at 5 mL min^{-1} flow rate although some non-hematite spherical particles, confirmed by Raman analysis, (~20-30 nm and ~1-2 nm in size) were observed.

Reproducibility of Synthesis. Reproducibility of the MWPF process was tested by repeating the fabrication of Hem-SSs two more times under the same experimental conditions using 0.1 mol L^{-1} $Fe(NO_3)_3.9H_2O$ precursor at 1 mL min^{-1} flow rate. Isolated Hem-SSs were characterized by TEM. In all cases TEM analyses showed ellipsoid Hem-SSs with particle size distribution of ~130 nm (length) and 80 nm (width), confirming that the developed synthesis method is reproducible and capable of producing Hem-SSs with similar size distributions (**Figure 5**).

View Article Online
DOI: 10.1039/C5GC02245B

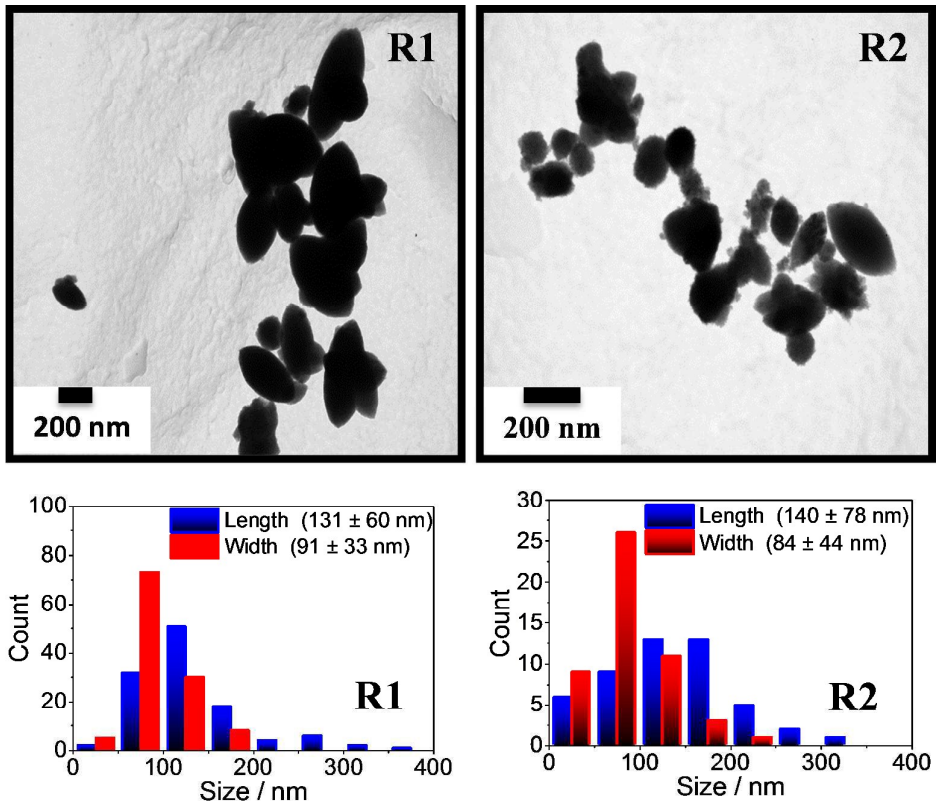

Figure 5 TEM images of ellipsoid Hem-SSs produced by two different repeat experiments (R1 and R2) under the same experimental conditions and the particle size distribution of the produced Hem-SSs.

Mechanism of Hem-SSs Formation. In agreement with previous literature,[8] the morphology of hematite particles is thought to be an oriented growth with primary nanoparticles. In general, mesocrystal formation mechanisms are described by the hierarchical self-assembly of primary nanoparticles following a non-classical crystallization route that is based on either self-assembly or ligand-directed assembly of well-aligned small nanoparticles.[1-4] During the formation of well-oriented superstructures, an equilibrium state is however essential between the interparticle interactions including the dipole-dipole attraction, van der Waals interaction and the double layer repulsion for directed self-assembly of colloidal particles.[28, 29] This type of balance can be facilitated by an external electric or magnetic field if sufficient dipole–dipole interactions are induced.[28, 29] In addition, self-assembly of nanostructures was also

View Article Online
DOI: 10.1039/C5GC02245B

shown in fluidic reactors that provide small reaction volumes and laminar flow, facilitating the fine-adjustment of mixing rates, shear forces and reagent concentrations.[30, 31]

Regarding the formation of ellipsoid Hem-SSs, the multiple effects induced by shear force due to fluid flow and continuously exerted microwave irradiation might have played the key roles, since no other templates/surfactants/organic solvents are present in our reaction system. The shear induced aggregation of nanoparticles can be described by the dimensionless Péclet number; shear forces have a stronger influence on aggregation for high flow Péclet numbers ($P_e \geq 1$).[30] The flow Péclet number for the dilute solutions of α-Fe_2O_3 NPs using particle size of ~10 nm (estimated by TEM) is 2.74×10^{-6}, suggesting that self-assembly of hematite primary particles was not probably due to shear induced aggregation.[30, 32] (***see ESI for calculations***)

Considering that no clear ellipsoid structures (**see ESI Figure S2 for TEM images**) formed when the conventional heating flow reactor was used, the self-assembly of primary hematite nanocrystals to form stable ellipsoid Hem-SSs is regarded to be induced by microwave irradiation (**Figure 6a-b**). The surprising effect of microwave heating on the oriented attachment of pre-synthesized α-Fe_2O_3 nanoparticles to form large and crystalline ellipsoidal α-Fe_2O_3 nanocrystals was also reported when in a batch reactor.[33] α-Fe_2O_3 nanoparticles are known to have magnetic moment that creates dipole–dipole attractions and they can act as antennas and absorb the microwave irradiation selectively.[34, 35] In an electromagnetic field generated by microwave irradiation, α-Fe_2O_3 nanoparticles are highly polarized and localized currents are probably created on the "hot surfaces" of α-Fe_2O_3 nanoparticles.[35]

In order to further understand the effect of microwave irradiation to ellipsoid Hem-SSs formation, control experiments were performed using a microwave batch reactor. In a typical control experiment, 3 mL of aqueous precursor solution (0.05, 0.1 and 0.2 mol L^{-1}

View Article Online
DOI: 10.1039/C5GC02245B

$Fe(NO_3)_3.9H_2O$) was irradiated by microwave for 6 min at 120 ^oC without stirring. At low concentration (0.05 mol L^{-1} $Fe(NO_3)_3.9H_2O$), particles could not be isolated. Hematites, characterised by UV-vis spectroscopy, were produced successfully when high concentration of precursor (0.1 and 0.2 mol L^{-1}) was used (**ESI Figure S5a**). Produced particles were isolated and further analysed by TEM. In contrast to ellipsoid Hem-SSs synthesized by MWPF system, few ellipsoid particles with irregular morphologies were produced by microwave batch reactor without stirring. (**ESI Figure S5b-f**), which is partially in agreement with the literature that reported ellipsoid α-Fe_2O_3 formation could take place under microwave heating in batch reactor.[33] It is also worth noting that ellipsoids were obviously formed at high precursor concentration in this study, indicating microwave irradiation can produce ellipsoid but the yield is relative moderate due to limited penetration depth of microwave in a batch reactor.

A microwave induced nucleation-aggregation mechanism followed by an oriented attachment of primary α-Fe_2O_3 nanoparticles and Oswald ripening may be proposed for the formation of Hem-SSs, although the exact mechanism of the formation at present remains unclear. As shown in **Figure 6b**, firstly goethite nanocrystals, α-FeO(OH) are probably generated by the microwave induced forced hydrolysis of $Fe(NO_3)_3.9H_2O$.[36, 37] Due to their high surface energy these freshly formed nanocrystals probably aggregate rapidly in a random manner and subsequently undergo dehydration to form primary α-Fe_2O_3 nanoparticles.[37] Meanwhile, microscopic "hot surfaces" created on particles probably accelerate the crystal growth. Produced primary nanoparticles are subsequently highly polarized under microwave irradiation (2.45 GHz) due to their excellent microwave absorbing characteristic and become energetically more excited.[34] Highly polarized activated primary α-Fe_2O_3 nanoparticles form due to generated dipole-dipole attractions[29] and start oriented attachment to produce Hem-SSs.[38-41] In addition, the smooth surface of ellipsoid Hem-SSs observed by TEM is thought

View Article Online
DOI: 10.1039/C5GC02245B

to be due to Oswald ripening after the oriented attachment of primary α-Fe_2O_3 nanoparticles.[36, 41] The oriented attachment process however leads to formation of ellipsoid Hem-SSs morphologies, which may be related to both the distortion of internal charges in nanoparticle crystal structure to polarize against the external field generated by microwave irradiation and the increased mass of assembled Hem-SSs that affects the particle motion under constant buoyant force of water. The reason behind the stability of hierarchical Hem-SSs formed and the absence of crystallographic fusion to single-crystals is still unknown. However, it could be attributed to both the shape of primary hematite nanoparticles and the residence time of Hem-SSs in the reactor and needs further investigation.

View Article Online
DOI: 10.1039/C5GC02245B

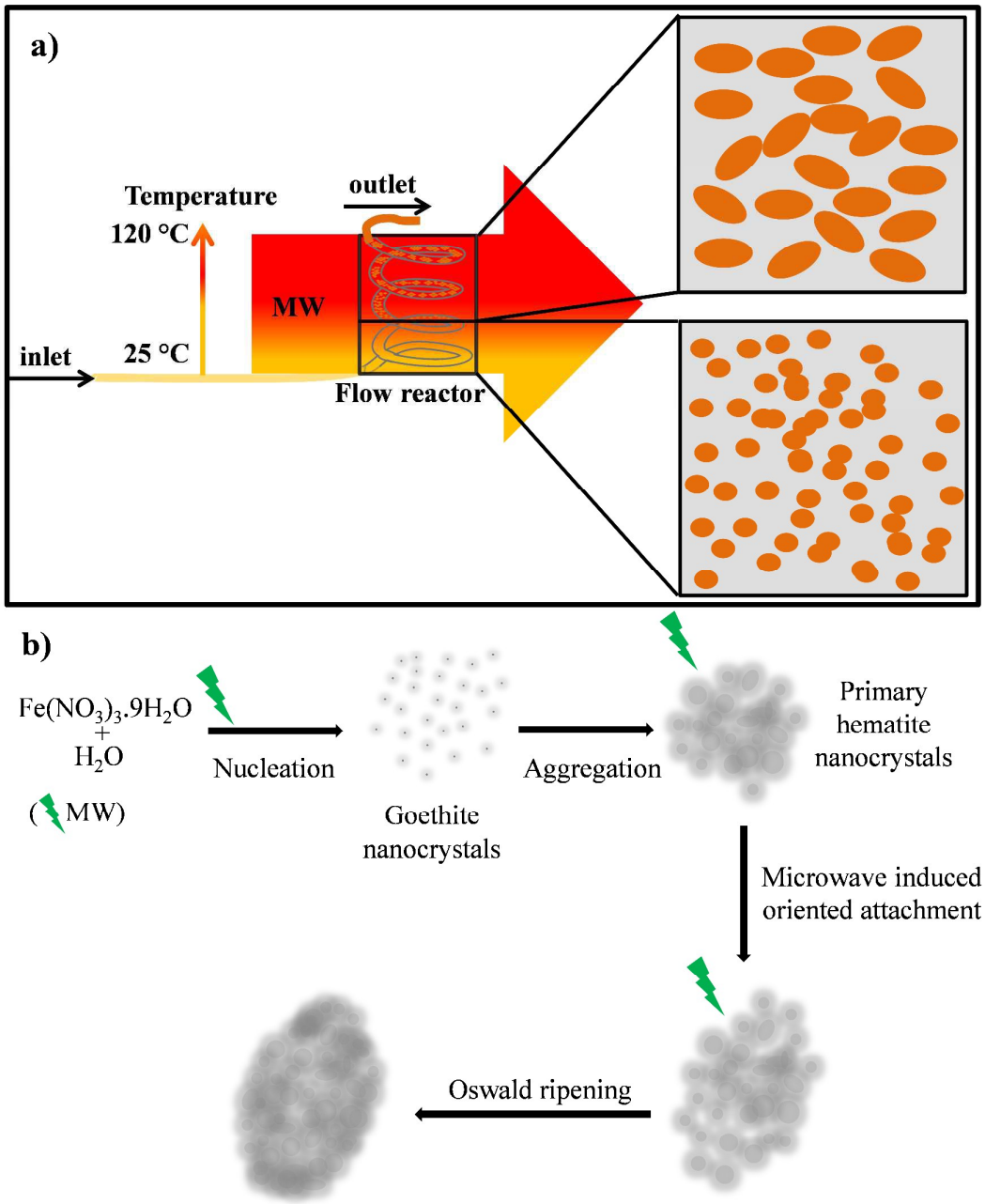

Figure 6 Schematic representation of proposed mechanism for microwave assisted directed self-assembly of primary hematite nanoparticles to form Hem-SSs. (**a**) Fabrication of primary hematite nanocrystals while travelling in the flow reactor (bottom square). Directed self-assembly of primary hematite nanoparticles under continuous microwave irradiation (top square). Colour change on the arrow (yellow to red) shows the possible temperature change throughout the flow reactor. (**b**) Proposed mechanism scheme for the formation of Hem-SSs.

View Article Online
DOI: 10.1039/C5GC02245B

Conclusions

Pure and crystalline ellipsoid hematite superstructures were fabricated in ~6 min time without employing surfactants or templates in a MWPF system using $Fe(NO_3)_3.9H_2O$ as the only precursor. Microwave irradiation is thought to direct the self-assembly of produced hematite subunits via selective heating and polarization of nanoparticles. Concentration and flow rate of the precursor solution were found to be critical for Hem-SS synthesis. Less crystalline hematite formation was observed at high precursor concentrations (0.1 and 0.2 mol L^{-1}). No hematite particle formation was observed at higher flow rates, indicating the significance of the amount of microwave energy absorbed per unit time. Conversely, CH was not able to produce pure hematite under identical conditions at 120 and even at 140 °C. The developed sustainable process that benefits from both MH and flow technology is reproducible and has the potential to fabricate other metal/metal oxide nanoparticles or their self-assembled superstructures, core/shell structures and hybrid nanomaterials.

Acknowledgements

We gratefully acknowledge the Leverhulme Trust (RPG-2012-582) for research funding.

References

1. R.-Q. Song and H. Cölfen, *Advanced Materials*, 2010, **22**, 1301-1330.
2. H. Cölfen and M. Antonietti, *Angew. Chem. Int. Ed.*, 2005, **44**, 5576-5591.
3. L. Bergström, E. V. Sturm, G. Salazar-Alvarez and H. Cölfen, *Accounts of Chemical Research*, 2015, **48**, 1391-1402.
4. M.-G. Ma and H. Cölfen, *Current Opinion in Colloid & Interface Science*, 2014, **19**, 56-65.
5. T. Tachikawa and T. Majima, *NPG Asia Mater*, 2014, **6**, e100.
6. X. Duan, L. Mei, J. Ma, Q. Li, T. Wang and W. Zheng, *Chemical Communications*, 2012, **48**, 12204-12206.
7. Z. An, J. Zhang, S. Pan and F. Yu, *The Journal of Physical Chemistry C*, 2009, **113**, 8092-8096.
8. X. Fei, W. Li, Z. Shao, S. Seeger, D. Zhao and X. Chen, *Journal of the American Chemical Society*, 2014, **136**, 15781-15786.
9. J. Ma, J. Teo, L. Mei, Z. Zhong, Q. Li, T. Wang, X. Duan, J. Lian and W. Zheng, *Journal of Materials Chemistry*, 2012, **22**, 11694-11700.
10. X.-L. Fang, C. Chen, M.-S. Jin, Q. Kuang, Z.-X. Xie, S.-Y. Xie, R.-B. Huang and L.-S. Zheng, *Journal of Materials Chemistry*, 2009, **19**, 6154-6160.

View Article Online
DOI: 10.1039/C5GC02245B

11. F. Jiao, J.-C. Jumas, M. Womes, A. V. Chadwick, A. Harrison and P. G. Bruce, *Journal of the American Chemical Society*, 2006, **128**, 12905-12909.
12. M. Zhu, Y. Wang, D. Meng, X. Qin and G. Diao, *Journal of Physical Chemistry C*, 2012, **116**, 16276-16285.
13. H.-J. Kim, K.-I. Choi, A. Pan, I.-D. Kim, H.-R. Kim, K.-M. Kim, C. W. Na, G. Cao and J.-H. Lee, *Journal of Materials Chemistry*, 2011, **21**, 6549-6555.
14. W. T. Dong and C. S. Zhu, *Journal of Materials Chemistry*, 2002, **12**, 1676-1683.
15. P. M. Kouotou, Z.-Y. Tian, H. Vieker and K. Kohse-Hoeinghaus, *Surface & Coatings Technology*, 2013, **230**, 59-65.
16. G. Qiu, H. Huang, H. Genuino, N. Opembe, L. Stafford, S. Dharmarathna and S. L. Suib, *The Journal of Physical Chemistry C*, 2011, **115**, 19626-19631.
17. A. Abou-Hassan, O. Sandre and V. Cabuil, *Angew. Chem. Int. Ed.*, 2010, **49**, 6268-6286.
18. M. Nishioka, M. Miyakawa, Y. Daino, H. Kataoka, H. Koda, K. Sato and T. M. Suzuki, *Industrial & Engineering Chemistry Research*, 2013, **52**, 4683-4687.
19. M. Nishioka, M. Miyakawa, H. Kataoka, H. Koda, K. Sato and T. M. Suzuki, *Nanoscale*, 2011, **3**, 2621-2626.
20. S. Horikoshi, H. Abe, K. Torigoe, M. Abe and N. Serpone, *Nanoscale*, 2010, **2**, 1441-1447.
21. S. Horikoshi, T. Sumi and N. Serpone, *Chemical Engineering and Processing: Process Intensification*, 2013, **73**, 59-66.
22. T. Fujii, F. M. F. de Groot, G. A. Sawatzky, F. C. Voogt, T. Hibma and K. Okada, *Physical Review B*, 1999, **59**, 3195-3202.
23. A. A. Tahir, K. G. U. Wijayantha, S. Saremi-Yarahmadi, M. Mazhar and V. McKee, *Chemistry of Materials*, 2009, **21**, 3763-3772.
24. D. A. Wheeler, G. Wang, Y. Ling, Y. Li and J. Z. Zhang, *Energy & Environmental Science*, 2012, **5**, 6682-6702.
25. K. Sivula, R. Zboril, F. Le Formal, R. Robert, A. Weidenkaff, J. Tucek, J. Frydrych and M. Grätzel, *Journal of the American Chemical Society*, 2010, **132**, 7436-7444.
26. D. L. A. de Faria, S. Venâncio Silva and M. T. de Oliveira, *Journal of Raman Spectroscopy*, 1997, **28**, 873-878.
27. M. Hanesch, *Geophysical Journal International*, 2009, **177**, 941-948.
28. J.-M. Meijer, D. V. Byelov, L. Rossi, A. Snigirev, I. Snigireva, A. P. Philipse and A. V. Petukhov, *Soft Matter*, 2013, **9**, 10729-10738.
29. M. Grzelczak, J. Vermant, E. M. Furst and L. M. Liz-Marzán, *ACS Nano*, 2010, **4**, 3591-3605.
30. C.-W. Wang, D. Sinton and M. G. Moffitt, *Journal of the American Chemical Society*, 2011, **133**, 18853-18864.
31. X. Zhang, K. D. Harris, N. L. Y. Wu, J. N. Murphy and J. M. Buriak, *ACS Nano*, 2010, **4**, 7021-7029.
32. J. Vermant and M. J. Solomon, *Journal of Physics: Condensed Matter*, 2005, **17**, R187.
33. W.-W. Wang, Y.-J. Zhu and M.-L. Ruan, *Journal of Nanoparticle Research*, 2007, **9**, 419-426.
34. T. Druzhinina, W. Weltjens, S. Hoeppener and U. S. Schubert, *Advanced Functional Materials*, 2009, **19**, 1287-1292.
35. X. Hu, J. C. Yu, J. Gong, Q. Li and G. Li, *Advanced Materials*, 2007, **19**, 2324-2329.
36. U. Schwertmann, J. Friedl and H. Stanjek, *Journal of Colloid and Interface Science*, 1999, **209**, 215-223.

View Article Online
DOI: 10.1039/C5GC02245B

37. J. F. Banfield, S. A. Welch, H. Zhang, T. T. Ebert and R. L. Penn, *Science*, 2000, **289**, 751-754.
38. M. Ocaña, M. P. Morales and C. J. Serna, *Journal of Colloid and Interface Science*, 1995, **171**, 85-91.
39. A. P. Alivisatos, *Science*, 2000, **289**, 736-737.
40. M. Adachi, Y. Murata, J. Takao, J. Jiu, M. Sakamoto and F. Wang, *Journal of the American Chemical Society*, 2004, **126**, 14943-14949.
41. Y. Cheng, Y. Wang, D. Chen and F. Bao, *The Journal of Physical Chemistry B*, 2005, **109**, 794-798.